

Contact Ion Pair Formation Is Not Necessarily Stronger than Solvent Shared Ion Pairing

Kenneth D. Judd, Nicole M. Gonzalez, Tinglu Yang, and Paul S. Cremer*



Cite This: *J. Phys. Chem. Lett.* 2022, 13, 923–930



Read Online

ACCESS |



Metrics & More

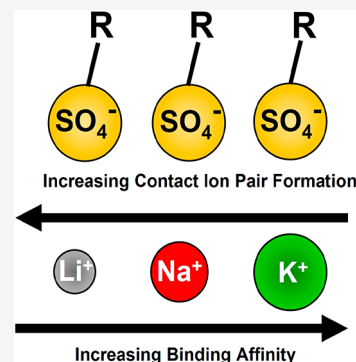


Article Recommendations



Supporting Information

ABSTRACT: Vibrational sum frequency spectroscopy (VSFS) and pressure–area Langmuir trough measurements were used to investigate the binding of alkali metal cations to eicosyl sulfate (ESO_4) surfactants in monolayers at the air/water interface. The number density of sulfate groups could be tuned by mixing the anionic surfactant with eicosanol. The equilibrium dissociation constant for K^+ to the fatty sulfate interface showed 10 times greater affinity than for Li^+ and approximately 3 times greater than for Na^+ . All three cations formed solvent shared ion pairs when the mole fraction of ESO_4 was 0.33 or lower. Above this threshold charge density, Li^+ formed contact ion pairs with the sulfate headgroups, presumably via bridging structures. By contrast, K^+ only bound to the sulfate moieties in solvent shared ion pairing configurations. The behavior for Na^+ was intermediate. These results demonstrate that there is not necessarily a correlation between contact ion pair formation and stronger binding affinity.



In 1921, Fajans reported that alkali metal cations (M^+) and halide anions with similar hydration enthalpies ($\Delta H_{\text{H}_{\text{yd}}}$) gave rise to sparingly soluble salts in water.^{1,2} As $\Delta H_{\text{H}_{\text{yd}}}$ for the cation and anion diverged, the corresponding salt was found to be more soluble. More recently, Collins proposed the Law of Matching Water Affinities (LMWA) as an extension of Fajans' observations to include biologically relevant ions, such as those that are pendant groups of polymers and proteins.^{3–6} He further suggested that contact ion pair formation should be more favorable between free cations and biologically relevant anionic functional groups with similar $\Delta H_{\text{H}_{\text{yd}}}$ or free energy of hydration ($\Delta G_{\text{H}_{\text{yd}}}$) values. By contrast, he hypothesized that solvent shared ion pairing would be expected if there were significant differences.

Numerous studies of specific alkali metal cation interactions with pendant carboxylate and sulfate groups have been performed for binding to micelles,^{7–15} polyelectrolytes,¹⁶ proteins,^{17,18} and monolayers.^{19–22} These investigations found that weakly hydrated cations paired better with pendant sulfate groups, while strongly hydrated cations paired better with carboxylate. Collins' hypothesis would suggest, for example, that K^+ would be more likely to form a contact ion pair with sulfate moieties compared with Li^+ because it binds more strongly and has a more similar $\Delta G_{\text{H}_{\text{yd}}}$ (Section S1). Unfortunately, previous studies have not addressed the question as to whether the binding to sulfate pendant groups occurs through solvent shared or contact pair formation. As such, it remains unknown as to whether contact pair formation is associated with stronger binding or not.

Herein, ion pairing was investigated with closely packed anionic monolayers of eicosyl sulfate (ESO_4) with LiCl , NaCl , and KCl in the subphase. Details concerning the experimental

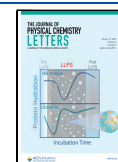
methods, fitting procedures, and fitting parameters are provided in Section S2. Vibrational sum frequency spectroscopy (VSFS) measurements of ordered water in the double layer confirmed the binding affinity order predicted by the LMWA. However, VSFS studies of the pendant sulfate $\nu_{\text{ss}}(\text{SO}_3^-)$ resonance revealed significant dehydration of a closely packed ESO_4 monolayer by Li^+ , but not by K^+ . Specifically, these results demonstrated an order of magnitude greater affinity for K^+ with ESO_4 monolayers compared to Li^+ . Nevertheless, Li^+ could bind through contact ion pair formation, while K^+ binding occurred through solvent shared ion pairing (Figure 1). Moreover, contact ion pairs between Li^+ and pendant sulfate occurred when two ESO_4 headgroups were packed closely enough together to allow Li^+ to bind bivalently. This finding does not support Collins' postulate regarding contact ion pair formation. Instead, it would appear that Li^+ has a greater propensity than larger cations to form contact ion pairs with sulfate and that ion hydration enthalpies and binding constants are not particularly useful indicators as to the mode of pairing.

In a first set of experiments, ESO_4 monolayers were formed at the air/aqueous solution interface on a Langmuir trough, and VSFS titrations in the OH stretch region were performed as a function of salt concentration (Figure 2A–C). The two

Received: November 1, 2021

Accepted: January 11, 2022

Published: January 20, 2022



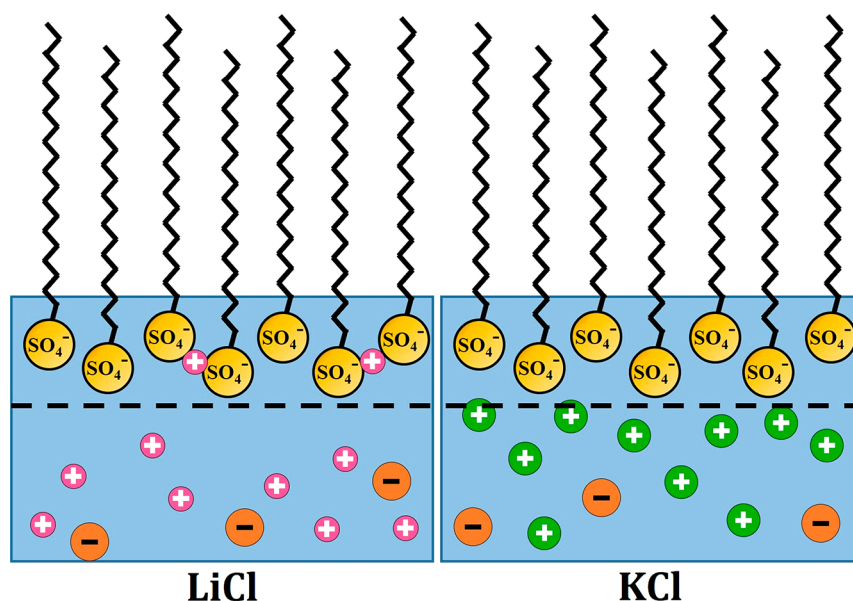


Figure 1. A densely packed ESO₄ monolayer displays opposite trends for cation specific binding and contact ion pair formation with alkali metal cations. K⁺ (green) pairs more strongly than Li⁺ (pink), yet strictly through solvent shared interactions, while Li⁺ can interact with the interface through contact ion pairing.

sharp peaks seen in the spectra at 2877 and 2941 cm⁻¹ correspond to the $\nu_{ss}(\text{CH}_3)$ and its Fermi resonance with the CH₃ bending mode, respectively, in agreement with previous studies.^{23–25} By contrast, the $\nu_{ss}(\text{CH}_2)$ peak at 2850 cm⁻¹ and the $\nu_{as}(\text{CH}_2)$ peak at 2920 cm⁻¹ from methylene groups were quite small. These results are consistent with the idea that all three monolayers were well packed and contained relatively few gauche conformations.^{26,27} Nevertheless, the methylene group signatures were lower over KCl solutions compared with NaCl and LiCl, indicating that the monolayer over KCl was relatively better ordered.

The OH stretch region between 3000 and 3800 cm⁻¹ gave rise to three much broader peaks. The two prominent OH stretch resonances near 3200 and 3400 cm⁻¹ represent water molecules beneath the negatively charged headgroups of the monolayer and should be oriented such that the hydrogen atoms face upward toward the negatively charged monolayer.^{25,28–31} These peaks correspond to water molecules with more (3200 cm⁻¹) and less (3400 cm⁻¹) tetrahedral ordering, respectively.^{32–34} A much smaller OH stretch resonance near 3600 cm⁻¹ represents water molecules situated just above the headgroup in a weaker hydrogen bonding environment.^{28,31,39} In this case, the water molecules are adjacent to the alkyl chains, and the hydrogen atoms face downward toward the bulk solution. This interpretation is consistent with previous spectra of highly charged anionic monolayers obtained by both heterodyne-detected VSFS (HD-VSFS)^{25,28,31} as well as computational results employing the maximum entropy method (MEM)³⁰ to extract the relative phase associated with each of the three peaks.

Interfacial water ordered by a charged surface can be separated into two populations.^{23,35,36,38,40–46} First, a chemically bound water population primarily interacts with the surface through hydrogen bonding. Second, a physically aligned water population is ordered by the electric field permeating into the solution from the interface.⁴⁰ At the surface charge density employed herein, nominally 0.7 C/m² without ion pairing (Section S7), the electric field-oriented

water dominates both the 3200 and the 3400 cm⁻¹ peaks.^{47,48}

Formation of ion pairs between cations in the subphase and the anionic functional groups present in the monolayer decrease the effective surface charge density and attenuate the VSFS signal in the OH stretch region. The extent of attenuation of the VSFS signal enables a quantitative comparison among the various cations that are employed.

The summed amplitudes of the 3200 and 3400 cm⁻¹ peaks are employed herein as a metric of ion affinity. It should be noted that the intensity of the 3600 cm⁻¹ peak is omitted from this analysis, as this peak was found to be relatively insensitive to the subphase environment under the conditions used herein. As can be seen, the 3200 and 3400 cm⁻¹ peaks decrease monotonically in each case while the adjacent CH peaks remain essentially unchanged. Ion specific effects are already present at 100 μM M⁺, with the intensity in the OH stretch region increasing in the order K⁺ < Na⁺ < Li⁺. The apparent equilibrium dissociation constants, $K_{D,app}$, were determined by fitting the normalized decrease in the VSFS amplitude of the 3200 and 3400 cm⁻¹ peak region to a Hill–Langmuir binding isotherm with a cooperativity coefficient, n (Figure 2D, inset).⁴⁹

$$I_{VSFS, Norm} = \frac{B_{max}[M^+]^n}{K_{D,app}^n + [M^+]^n} \quad (1)$$

As can be seen, the value of n is less than 1 in each case, which indicates that the binding is anticooperative.⁴⁹ Indeed, decreasing affinity should be expected because of charge neutralization. While binding between a charged group at the surface and a cation in solution decreases the surface potential, increasing ionic strength also lowers the surface potential through screening of the interfacial electric field.⁵⁰ Both processes lead to a decrease in the VSFS signal in the OH region.^{35,51} As such, the $K_{D,app}$ values are apparent binding constants that arise from a combination of binding and screening. Nevertheless, K⁺ should have a binding affinity that is 10 times stronger than Li⁺ and about 3 times stronger than

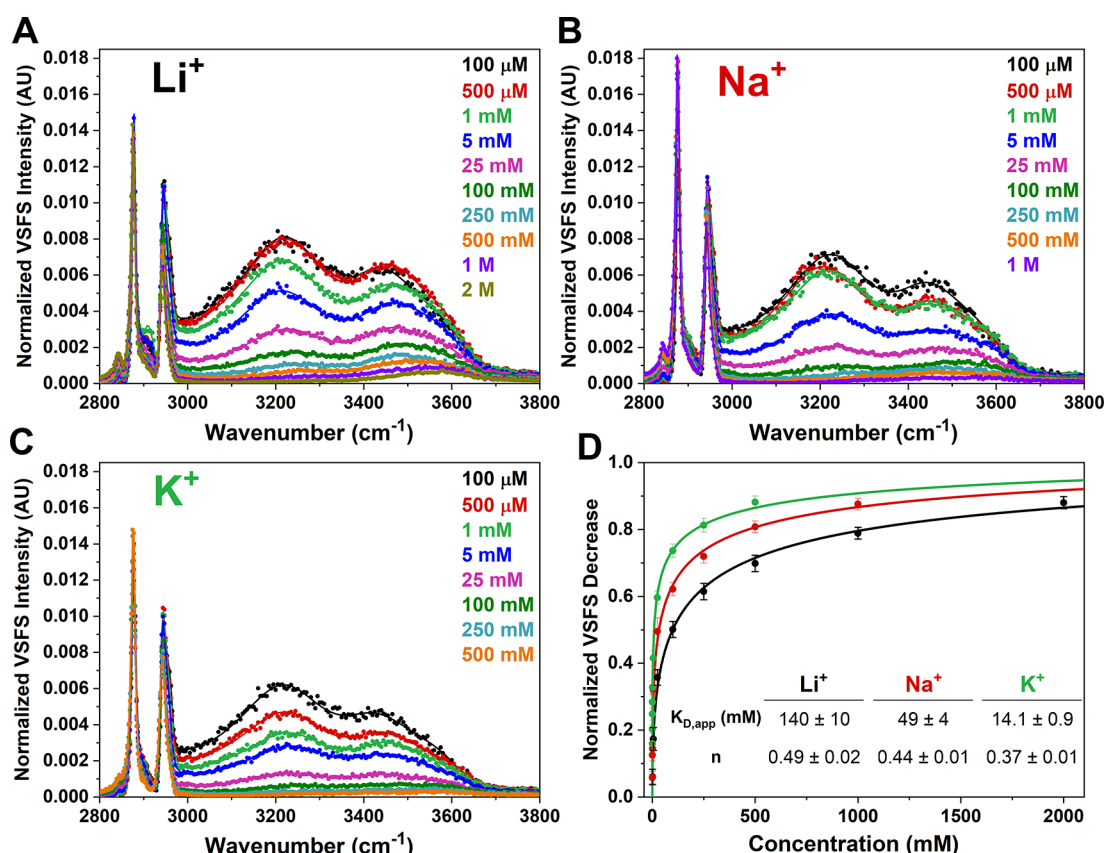


Figure 2. VSFS spectra in the OH stretch region of an ESO₄ monolayer over subphases containing (A) LiCl/LiOH, (B) NaCl/NaOH, and (C) KCl/KOH at a constant mean molecular area (MMA) of 23 ± 1 Å² with the SSP polarization combinations. The MMA was determined from Langmuir trough pressure–area (Π –A) isotherms (Section S3). All subphases contained 100 μM MOH with enough MCl added to achieve the listed alkali metal ion concentrations. In all cases where the salt concentration was ≥ 1 mM, 4 μM EDTA was included to chelate trace metal contaminants. The pH determined after each experiment was 9.3 ± 0.1 for all conditions at 21 ± 1 °C. At this pH, the monolayers were fully deprotonated (Section S4). The colored circles are experimental data points representing the average of at least three trials, and the solid lines are fits to the spectra. (D) Relative decrease in the summed amplitudes of the 3200 and 3400 cm⁻¹ peaks are presented as colored circles. These data were fit to binding isotherms with the corresponding dissociation constants and cooperativity terms listed in the inset table. Additional details for the binding isotherm fitting procedures are provided in Section S5. The effect of interference at salt concentrations < 100 μM is described in Section S6.^{35–38}

Na⁺. Integration of Langmuir trough surface pressure–area (Π –A) isotherms confirmed the $K^+ > Na^+ > Li^+$ affinity order for ESO₄ monolayers (Section S8).

The data in Figure 2 and Section S8 demonstrated that the affinity of cations for packed ESO₄ monolayers follows the LMWA prediction.^{3–6} Unfortunately, neither Π –A isotherm measurements nor VSFS measurements in the OH stretch region provide direct insight as to whether alkali metal cations bind to the surfactant headgroups via contact ion pair formation or through solvent shared ion pairing. To obtain this information, VSFS spectra of the $\nu_{ss}(\text{SO}_3^-)$ mode of ESO₄ monolayers were obtained in the presence of increasing subphase concentration of LiCl, NaCl, and KCl (Figure 3A–C). The hydrated $\nu_{ss}(\text{SO}_3^-)$ mode from a densely packed dodecyl sulfate monolayer occurs at ~ 1070 cm⁻¹.⁵² Hydration of these negatively charged functional groups transfers a small amount of electron density into the hydrating water molecules, which red shifts the vibrational mode to lower frequency relative to the gas phase peak or the one obtained with the solid salt.^{53,54} Contact ion pairs partially dehydrate the anionic functional group. However, alkali metal cations cannot accept excess electron density. As such, the frequency shifts back

toward the blue upon contact ion pair formation with these metal cations.^{22,55–61}

The center frequency for the fitted data in Figure 3A–C is plotted in Figure 3D with the fitting parameters for 250 mM salt in Table 1. The spectra over LiCl subphases required 2 peaks to fit the data, while the other spectra could be fit to a single peak. As can be seen, the center of mass for the Li⁺ spectra already shifted to higher frequency by introducing 100 μM of the corresponding hydroxide salt, and two distinct peaks were evident. The high frequency peak grew continuously up to 250 mM LiCl, after which point little additional spectral changes were observed. The high frequency peak was blue-shifted by approximately 25 cm⁻¹ with respect to the reference peak over neat water as it approached the saturation point. By contrast, the lower frequency peak was blue-shifted by 12 cm⁻¹ at the highest concentration, and this shift occurred over the entire concentration range. Next, the Na⁺ peak blue-shifted only 4 cm⁻¹ with respect to the reference peak. Moreover, the resonance frequency stopped changing by 100 mM NaCl. Finally, the peak associated with K⁺ maintained a center frequency within ± 1 cm⁻¹ of the reference peak over the entire concentration range. Nevertheless, this peak markedly increased in intensity and narrowed as KOH/KCl was

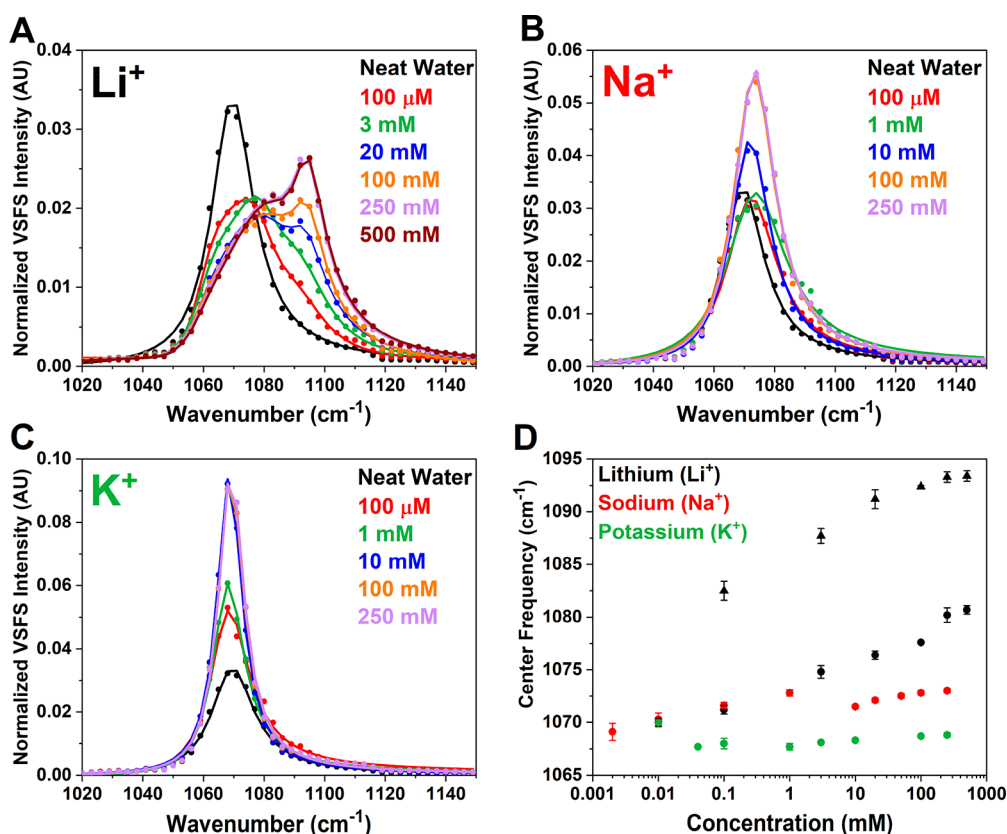


Figure 3. VSFS spectra of the $\nu_{ss}(\text{SO}_3^-)$ resonance from an ESO_4 monolayer over a subphase containing (A) LiCl/LiOH , (B) NaCl/NaOH , and (C) KCl/KOH at an MMA of $23 \pm 1 \text{ \AA}^2$ with the SSP polarization combination. The MMA was determined from Langmuir trough pressure–area (Π – A) isotherms (Section S3). All subphases contained $100 \mu\text{M}$ MOH with sufficient MCl to achieve the desired alkali metal ion concentration. In all cases where the salt concentration was $\geq 1 \text{ mM}$, $4 \mu\text{M}$ EDTA was included to chelate trace metal contaminants. All experiments were run at $21 \pm 1 \text{ }^\circ\text{C}$ and $\text{pH } 9.3 \pm 0.1$. The colored circles are experimental data points representing the average of at least 3 trials, and the solid lines are fits to the spectra. (D) The center frequency of the spectral features is plotted against the cation concentration. For Li^+ , the higher frequency peak is plotted with triangles, and the lower frequency peak is plotted with circles. “Neat water” actually contains $2 \mu\text{M}$ Na^+ , due to its presence in the NaESO_4 salt used to form the monolayer, and this data point is therefore plotted with the rest of the sodium data. Additional spectra are provided in Section S9. Additional analysis, including spectral measurement in PPP and SPS polarization, is provided in Section S10.

Table 1. Fitting Parameters for $\nu_{ss}(\text{SO}_3^-)$ Resonance over 250 mM MCl with the Standard Deviation in Parentheses

	neat water	LiCl	NaCl	KCl
center frequency (ω_n , cm^{-1})	1069.1 (0.8)	1081.5 (0.7) ^a 1093.7 (0.4) ^b	1073.2 (0.1)	1068.7 (0.1)
half-width at half-maximum (Γ , cm^{-1})	8.4 (0.3)	18 (1) ^a 6.6 (0.8) ^b	8.1 (0.2)	5.1 (0.1)

^aLow frequency peak. ^bHigh frequency peak.

added. This is consistent with an increase in environmental homogeneity of the pendant sulfate group at constant MMA when K^+ is present in the subphase relative to Na^+ or Li^+ .^{62,63} The same intensity trend is seen in the antisymmetric stretching mode (Section S10). It is also consistent with the relatively small methylene signatures over K^+ subphases found in Figure 2C. The peak shifts observed herein are surprising, as dehydration of pendant sulfate groups through contact ion pair formation follows the order $\text{Li}^+ > \text{Na}^+ > \text{K}^+$. This is opposite to the trend for the thermodynamic binding measurements in Figure 2 and Section S8. Also, changing the identity of the anion from Cl^- to OH^- had no noticeable effect on these results (Section S11).

In a final set of experiments, the influence of the surface charge density on the nature of ion pairing between the alkali metal cations and the ESO_4 monolayer was explored by

replacing some of the fatty sulfate groups with fatty alcohols. VSFS data from the $\nu_{ss}(\text{SO}_3^-)$ mode of these mixed monolayers was collected over 250 mM LiCl , NaCl , and KCl at ESO_4 mole fractions (χ_{ESO_4}) of 0.20, 0.33, and 0.50 (Figure 4). As can be seen, there was little difference in the peak position or line shape among the cations at 0.20 and 0.33 χ_{ESO_4} , and no indication of either ion specific dehydration or contact ion pair formation was found. However, the $\nu_{ss}(\text{SO}_3^-)$ spectra at 0.50 χ_{ESO_4} revealed significant dehydration of the pendant sulfate group when Li^+ was present in the subphase. A modest peak shift was also observed for Na^+ in comparison with K^+ . As such, the 0.50 χ_{ESO_4} spectra resembled the data obtained with pure ESO_4 monolayers (Figure 3).

For hexagonal packing, a 0.33 χ_{ESO_4} monolayer is the highest concentration that would still allow every pendant sulfate to be completely surrounded by alcohol functional groups (Figure

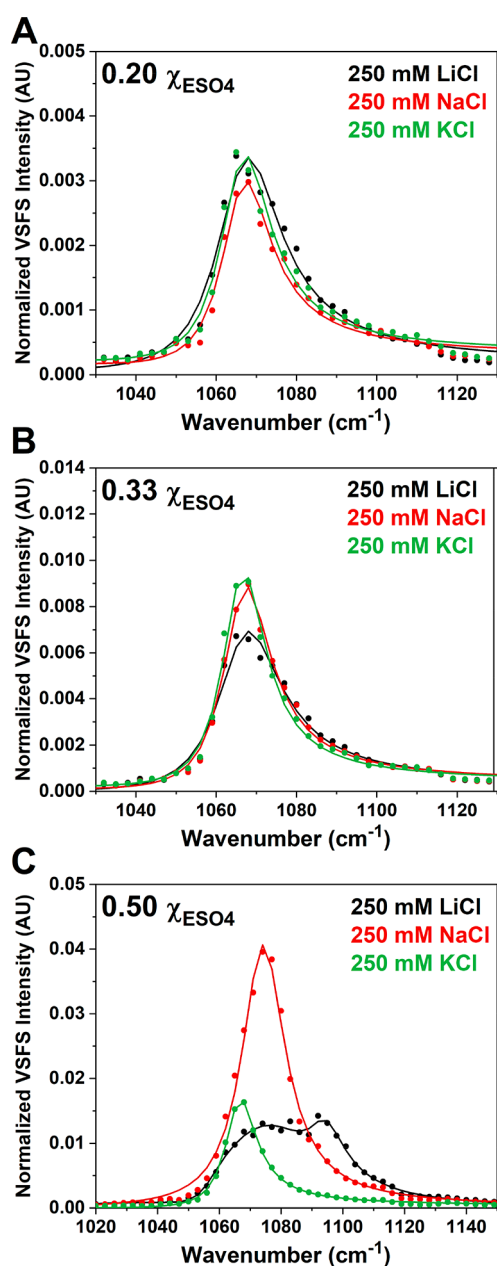


Figure 4. VSFS spectra of $\nu_{ss}(\text{SO}_3^-)$ resonance from mixed monolayers of ESO_4 and eicosanol at (A) 0.20 χ_{ESO_4} , (B) 0.33 χ_{ESO_4} , and (C) 0.50 χ_{ESO_4} at an MMA of $21 \pm 0.5 \text{ \AA}^2$ with the SSP polarization combination. The subphase contains 250 mM MCl and 100 μM MOH of the corresponding alkali metal hydroxide, in addition to 4 μM EDTA to chelate trace metal contaminants. The pH was 9.3 ± 0.1 at a temperature of $21 \pm 1^\circ\text{C}$ under all conditions. The colored circles are experimental data points representing the average of at least three trials, and the solid lines are fits to the spectra. Additional details are provided in Section S12.

5). Such isolation of the sulfate headgroups may be expected to occur since they are negatively charged and will repel each other. Moreover, since contact ion pair formation was not observed with LiCl at 0.33 χ_{ESO_4} , contact ion pairing between Li^+ and pendant sulfate presumably involves the bridging of adjacent headgroups by metal ions (Figure 1).

In contrast to the results herein, fatty carboxylate monolayer systems show the same trend for binding and contact ion pair formation with the same alkali metal cations. Specifically, Li^+

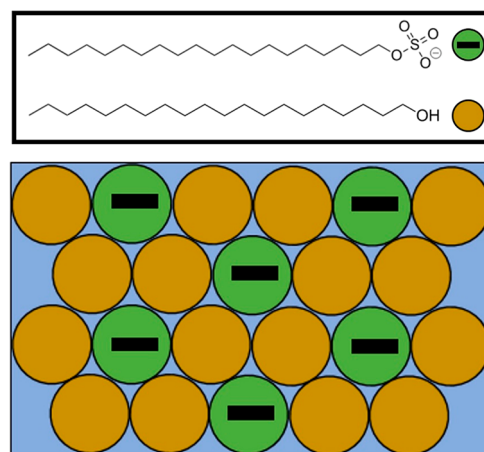


Figure 5. Overhead view of a mixed monolayer of ESO_4 and eicosanol at 0.33 χ_{ESO_4} .

binds the strongest^{14,16} and has the greatest propensity to form contact ion pairs.²² We performed a parallel set of studies with arachidic acid and found the binding constant and contact pair trends both followed the order $\text{Li}^+ > \text{Na}^+ > \text{K}^+$ (Section S13). Since different systems can exhibit opposite trends, the question naturally arises as to when contact pairing versus solvent shared pairing should be expected. Ion pairing in aqueous solutions is a relatively complex process compared to the analogous pairing process in the absence of water. Moreover, the gas phase interaction between Li^+ and the sulfate headgroup should be more free energy favorable than for K^+ , as Li^+ can sit closer to the anion. At the air/water interface, however, K^+ has a substantially greater affinity for sulfate. In aqueous solutions, both the cation and the anion may shed hydration water during the binding process. These hydration waters are then released into the bulk solution where new water–water interactions are formed. Typically, there are free energy costs associated with shedding hydration water around each ion and free energy gains associated with the ion pairing event as well as with the formation of new water–water interactions.

When K^+ interacts with sulfate, the free energy dehydration penalty for removing water from around the cation should be smaller than with Li^+ , since the ion pairing interaction only involves solvent shared pairing. Moreover, K^+ is a larger ion that holds its waters less tightly. Nevertheless, the additional dehydration penalty is paid in the Li^+ system since a stronger contact pair can be formed. The dehydration costs associated with contact pair formation with Li^+ , however, are sufficiently high that the dissociation constant between Li^+ and sulfate is weaker. Li^+ only pays this cost when it is able to bridge two sulfate moieties. One possible reason for this could be the need to displace fewer hydration waters in a bridging geometry compared with one-to-one contact pair formation. Indeed, some hydration water between the anionic headgroups is already released through the compression of the monolayer by the trough barriers.

Since the work herein does not support the idea that stronger binding necessarily means contact pair formation, it might be tempting to conclude that smaller cations have a higher propensity to form contact pairs when the anion identity is kept constant. Indeed, the free energy gain with smaller cations should be enthalpically more favorable. However, there are counterexamples in the literature where

it has been found that larger cations more easily form contact pairs with a common anion compared with smaller cations. For example, Ca^{2+} bridges phosphate moieties between adjacent phosphate groups on phosphatidylinositol 4,5-bisphosphate ($\text{PI}(4,5)\text{P}_2$) lipids in biomembranes, while the smaller Mg^{2+} ion forms more solvent shared structures.⁶¹ Undoubtedly, a general model for contact pairing in aqueous solutions will ultimately need to consider the hydration thermodynamics and the charge, as well as the chemical structure of the ions. Indeed, these are the same parameters that Fajans originally suggested would be decisive for predicting the solubility of salts 100 years ago.² In addition to these ideas, multivalency and the spatial positioning of the ions can also be decisive as indicated by the data in Figure 4.

In summary, the work herein demonstrates that stronger ion affinity does not necessarily correlate with a greater propensity to form contact ion pairs. Although the equilibrium dissociation constant for K^+ to pendant sulfate headgroups is an order of magnitude stronger than for Li^+ (Figure 2), K^+ interacts with the sulfate moiety exclusively through solvent shared interactions (Figure 3C). By contrast, Li^+ can form contact ion pairs above a threshold ESO_4 surface density (Figures 3A and 4C). This is significant, as it reveals specific circumstances under which contact ion pair formation does not follow the same order as the dissociation constant but instead follows a reverse trend.

■ ASSOCIATED CONTENT

Supporting Information

The Supporting Information is available free of charge at <https://pubs.acs.org/doi/10.1021/acs.jpclett.1c03576>.

Thermodynamic hydration values, materials and methods, VSFS fitting ranges, Π -A isotherms for all conditions, deprotonation of monolayers, binding constant fitting, interference of VSFS signal at low ionic strength, surface charge density calculations, compression free energy of Π -A isotherms, additional VSFS spectra of the $\nu_{\text{ss}}(\text{SO}_3^-)$ resonance, plotted fit parameters of the $\nu_{\text{ss}}(\text{SO}_3^-)$ resonance, SPS and PPP polarization combination VSFS spectra of the $\nu_{\text{ss}}(\text{SO}_3^-)$ resonance, interaction of MOH and ESO_4 , Π -A isotherms for mixed ESO_4 /eicosanol monolayers, plotted fit parameters for the $\nu_{\text{ss}}(\text{SO}_3^-)$ resonance of mixed ESO_4 /eicosanol monolayers, interaction of MOH and arachidic acid, and MATLAB fitting parameters with error ranges for all the VSFS spectra (PDF)

■ AUTHOR INFORMATION

Corresponding Author

Paul S. Cremer – Department of Chemistry and Department of Biochemistry and Molecular Biology, The Pennsylvania State University, University Park, Pennsylvania 16802, United States; orcid.org/0000-0002-8524-0438; Email: psc11@psu.edu

Authors

Kenneth D. Judd – Department of Chemistry, The Pennsylvania State University, University Park, Pennsylvania 16802, United States; orcid.org/0000-0003-3980-6960

Nicole M. Gonzalez – Department of Chemistry, The Pennsylvania State University, University Park, Pennsylvania 16802, United States

Tinglu Yang – Department of Chemistry, The Pennsylvania State University, University Park, Pennsylvania 16802, United States; orcid.org/0000-0003-0872-8218

Complete contact information is available at: <https://pubs.acs.org/doi/10.1021/acs.jpclett.1c03576>

Notes

The authors declare no competing financial interest.

■ ACKNOWLEDGMENTS

The authors thank the National Science Foundation (CHE-2004050) for support.

■ REFERENCES

- (1) Fajans, K. Löslichkeit und Ionisation vom Standpunkte der Atomstruktur. *Naturwissenschaften* **1921**, 9 (37), 729–738.
- (2) Fajans, K.; Karagunis, G. Osmotisches Verhalten von Starken Elektrolyten in Lösung Und Hydratation Ihrer Ionen. *Angew. Chem.* **1930**, 43 (48), 1046–1048.
- (3) Collins, K. D. Ions from the Hofmeister Series and Osmolytes: Effects on Proteins in Solution and in the Crystallization Process. *Methods* **2004**, 34 (3), 300–311.
- (4) Collins, K. D. Ion Hydration: Implications for Cellular Function, Polyelectrolytes, and Protein Crystallization. *Biophys. Chem.* **2006**, 119 (3), 271–281.
- (5) Collins, K. D.; Neilson, G. W.; Enderby, J. E. Ions in Water: Characterizing the Forces That Control Chemical Processes and Biological Structure. *Biophys. Chem.* **2007**, 128 (2), 95–104.
- (6) Collins, K. D. Why Continuum Electrostatics Theories Cannot Explain Biological Structure, Polyelectrolytes or Ionic Strength Effects in Ion–Protein Interactions. *Biophys. Chem.* **2012**, 167, 43–59.
- (7) Ropers, M. H.; Czichocki, G.; Brezesinski, G. Counterion Effect on the Thermodynamics of Micellization of Alkyl Sulfates. *J. Phys. Chem. B* **2003**, 107 (22), 5281–5288.
- (8) Feinstein, M. E.; Rosano, H. L. The Determination of the Apparent Binding of Counterions to Micelles by Electromotive Force Measurements. *J. Colloid Interface Sci.* **1967**, 24 (1), 73–79.
- (9) Jäger, C. M.; Hirsch, A.; Schade, B.; Böttcher, C.; Clark, T. Counterions Control the Self-Assembly of Structurally Persistent Micelles: Theoretical Prediction and Experimental Observation of Stabilization by Sodium Ions. *Chem. Weinh. Bergstr. Ger.* **2009**, 15 (34), 8586–8592.
- (10) Missel, P. J.; Mazer, N. A.; Carey, M. C.; Benedek, G. B. Influence of Alkali-Metal Counterion Identity on the Sphere-to-Rod Transition in Alkyl Sulfate Micelles. *J. Phys. Chem.* **1989**, 93 (26), 8354–8366.
- (11) Mukerjee, P.; Mysels, K.; Kapauan, P. Counterion Specificity in the Formation of Ionic Micelles - Size, Hydration, and Hydrophobic Bonding Effects. *J. Phys. Chem.* **1967**, 71 (13), 4166–4175.
- (12) Lu, J. R.; Marrocco, A.; Su, T. J.; Thomas, R. K.; Penfold, J. Adsorption of Dodecyl Sulfate Surfactants with Monovalent Metal Counterions at the Air-Water Interface Studied by Neutron Reflection and Surface Tension. *J. Colloid Interface Sci.* **1993**, 158 (2), 303–316.
- (13) Renoncourt, A.; Vlachy, N.; Bauduin, P.; Drechsler, M.; Touraud, D.; Verbavatz, J.-M.; Dubois, M.; Kunz, W.; Ninham, B. W. Specific Alkali Cation Effects in the Transition from Micelles to Vesicles through Salt Addition. *Langmuir* **2007**, 23 (5), 2376–2381.
- (14) Vlachy, N.; Drechsler, M.; Verbavatz, J.-M.; Touraud, D.; Kunz, W. Role of the Surfactant Headgroup on the Counterion Specificity in the Micelle-to-Vesicle Transition through Salt Addition. *J. Colloid Interface Sci.* **2008**, 319 (2), 542–548.
- (15) Vlachy, N.; Jagoda-Cwiklik, B.; Vácha, R.; Touraud, D.; Jungwirth, P.; Kunz, W. Hofmeister Series and Specific Interactions of Charged Headgroups with Aqueous Ions. *Adv. Colloid Interface Sci.* **2009**, 146 (1), 42–47.

- (16) Kherb, J.; Flores, S. C.; Cremer, P. S. Role of Carboxylate Side Chains in the Cation Hofmeister Series. *J. Phys. Chem. B* **2012**, *116* (25), 7389–7397.
- (17) Beierlein, F. R.; Clark, T.; Braunschweig, B.; Engelhardt, K.; Glas, L.; Peukert, W. Carboxylate Ion Pairing with Alkali-Metal Ions for β -Lactoglobulin and Its Role on Aggregation and Interfacial Adsorption. *J. Phys. Chem. B* **2015**, *119* (17), 5505–5517.
- (18) Heyda, J.; Pokorná, J.; Vrbka, L.; Vácha, R.; Jagoda-Cwiklik, B.; Konvalinka, J.; Jungwirth, P.; Vondrášek, J. Ion Specific Effects of Sodium and Potassium on the Catalytic Activity of HIV-1 Protease. *Phys. Chem. Chem. Phys. PCCP* **2009**, *11* (35), 7599–7604.
- (19) Weißenborn, E.; Braunschweig, B. Specific Ion Effects of Dodecyl Sulfate Surfactants with Alkali Ions at the Air–Water Interface. *Molecules* **2019**, *24* (16), 2911.
- (20) Goddard, E. D.; Kao, O.; Kung, H. C. Counterion Effects in Charged Monolayers. *J. Colloid Interface Sci.* **1968**, *27* (4), 616–624.
- (21) Peng, M.; Duignan, T. T.; Nguyen, A. V. Quantifying the Counterion-Specific Effect on Surfactant Adsorption Using Modeling, Simulation, and Experiments. *Langmuir* **2020**, *36* (43), 13012–13022.
- (22) Sthoer, A.; Hladíková, J.; Lund, M.; Tyrode, E. Molecular Insight into Carboxylic Acid–Alkali Metal Cations Interactions: Reversed Affinities and Ion-Pair Formation Revealed by Non-Linear Optics and Simulations. *Phys. Chem. Chem. Phys.* **2019**, *21* (21), 11329–11344.
- (23) Gragson, D. E.; McCarty, B. M.; Richmond, G. L. Ordering of Interfacial Water Molecules at the Charged Air/Water Interface Observed by Vibrational Sum Frequency Generation. *J. Am. Chem. Soc.* **1997**, *119* (26), 6144–6152.
- (24) Guyot-Sionnest, P.; Hunt, J. H.; Shen, Y. R. Sum-Frequency Vibrational Spectroscopy of a Langmuir Film: Study of Molecular Orientation of a Two-Dimensional System. *Phys. Rev. Lett.* **1987**, *59* (14), 1597–1600.
- (25) Mondal, J. A.; Nihonyanagi, S.; Yamaguchi, S.; Tahara, T. Structure and Orientation of Water at Charged Lipid Monolayer/Water Interfaces Probed by Heterodyne-Detected Vibrational Sum Frequency Generation Spectroscopy. *J. Am. Chem. Soc.* **2010**, *132* (31), 10656–10657.
- (26) Lambert, A. G.; Davies, P. B.; Neivandt, D. J. Implementing the Theory of Sum Frequency Generation Vibrational Spectroscopy: A Tutorial Review. *Appl. Spectrosc. Rev.* **2005**, *40* (2), 103–145.
- (27) Gurau, M. C.; Castellana, E. T.; Albertorio, F.; Kataoka, S.; Lim, S.-M.; Yang, R. D.; Cremer, P. S. Thermodynamics of Phase Transitions in Langmuir Monolayers Observed by Vibrational Sum Frequency Spectroscopy. *J. Am. Chem. Soc.* **2003**, *125* (37), 11166–11167.
- (28) Nojima, Y.; Suzuki, Y.; Yamaguchi, S. Weakly Hydrogen-Bonded Water Inside Charged Lipid Monolayer Observed with Heterodyne-Detected Vibrational Sum Frequency Generation Spectroscopy. *J. Phys. Chem. C* **2017**, *121* (4), 2173–2180.
- (29) Nihonyanagi, S.; Yamaguchi, S.; Tahara, T. Direct Evidence for Orientational Flip-Flop of Water Molecules at Charged Interfaces: A Heterodyne-Detected Vibrational Sum Frequency Generation Study. *J. Chem. Phys.* **2009**, *130* (20), 204704.
- (30) Pullanchery, S.; Yang, T.; Cremer, P. S. Introduction of Positive Charges into Zwitterionic Phospholipid Monolayers Disrupts Water Structure Whereas Negative Charges Enhances It. *J. Phys. Chem. B* **2018**, *122* (51), 12260–12270.
- (31) Sartin, M. M.; Sung, W.; Nihonyanagi, S.; Tahara, T. Molecular Mechanism of Charge Inversion Revealed by Polar Orientation of Interfacial Water Molecules: A Heterodyne-Detected Vibrational Sum Frequency Generation Study. *J. Chem. Phys.* **2018**, *149* (2), 024703.
- (32) Kim, J.; Kim, G.; Cremer, P. S. Investigations of Polyelectrolyte Adsorption at the Solid/Liquid Interface by Sum Frequency Spectroscopy: Evidence for Long-Range Macromolecular Alignment at Highly Charged Quartz/Water Interfaces. *J. Am. Chem. Soc.* **2002**, *124* (29), 8751–8756.
- (33) Tian, C. S.; Shen, Y. R. Structure and Charging of Hydrophobic Material/Water Interfaces Studied by Phase-Sensitive Sum-Frequency Vibrational Spectroscopy. *Proc. Natl. Acad. Sci. U. S. A.* **2009**, *106* (36), 15148–15153.
- (34) Du, Q.; Freysz, E.; Shen, Y. R. Surface Vibrational Spectroscopic Studies of Hydrogen Bonding and Hydrophobicity. *Science* **1994**, *264* (5160), 826–828.
- (35) Wen, Y.-C.; Zha, S.; Liu, X.; Yang, S.; Guo, P.; Shi, G.; Fang, H.; Shen, Y. R.; Tian, C. Unveiling Microscopic Structures of Charged Water Interfaces by Surface-Specific Vibrational Spectroscopy. *Phys. Rev. Lett.* **2016**, *116* (1), 016101.
- (36) Gonella, G.; Lütgebaucks, C.; de Beer, A. G. F.; Roke, S. Second Harmonic and Sum-Frequency Generation from Aqueous Interfaces Is Modulated by Interference. *J. Phys. Chem. C* **2016**, *120* (17), 9165–9173.
- (37) Ohno, P. E.; Saslow, S. A.; Wang, H.; Geiger, F. M.; Eienthal, K. B. Phase-Referenced Nonlinear Spectroscopy of the α -Quartz/Water Interface. *Nat. Commun.* **2016**, *7* (1), 13587.
- (38) Ohno, P. E.; Wang, H.; Geiger, F. M. Second-Order Spectral Lineshapes from Charged Interfaces. *Nat. Commun.* **2017**, *8* (1), 1032.
- (39) Chen, X.; Hua, W.; Huang, Z.; Allen, H. C. Interfacial Water Structure Associated with Phospholipid Membranes Studied by Phase-Sensitive Vibrational Sum Frequency Generation Spectroscopy. *J. Am. Chem. Soc.* **2010**, *132* (32), 11336–11342.
- (40) Ong, S.; Zhao, X.; Eienthal, K. B. Polarization of Water Molecules at a Charged Interface: Second Harmonic Studies of the Silica/Water Interface. *Chem. Phys. Lett.* **1992**, *191* (3), 327–335.
- (41) Jena, K. C.; Covert, P. A.; Hore, D. K. The Effect of Salt on the Water Structure at a Charged Solid Surface: Differentiating Second- and Third-Order Nonlinear Contributions. *J. Phys. Chem. Lett.* **2011**, *2* (9), 1056–1061.
- (42) Dalstein, L.; Chiang, K.-Y.; Wen, Y.-C. Direct Quantification of Water Surface Charge by Phase-Sensitive Second Harmonic Spectroscopy. *J. Phys. Chem. Lett.* **2019**, *10* (17), 5200–5205.
- (43) Rehl, B.; Rashwan, M.; DeWalt-Kerian, E. L.; Jarisz, T. A.; Darlington, A. M.; Hore, D. K.; Gibbs, J. M. New Insights into $\chi^{(3)}$ Measurements: Comparing Nonresonant Second Harmonic Generation and Resonant Sum Frequency Generation at the Silica/Aqueous Electrolyte Interface. *J. Phys. Chem. C* **2019**, *123* (17), 10991–11000.
- (44) Urashima, S.; Myalitsin, A.; Nihonyanagi, S.; Tahara, T. The Topmost Water Structure at a Charged Silica/Aqueous Interface Revealed by Heterodyne-Detected Vibrational Sum Frequency Generation Spectroscopy. *J. Phys. Chem. Lett.* **2018**, *9* (14), 4109–4114.
- (45) Pezzotti, S.; Galimberti, D. R.; Shen, Y. R.; Gaigeot, M.-P. Structural Definition of the BIL and DL: A New Universal Methodology to Rationalize Non-Linear $\chi^{(2)}$ (ω) SFG Signals at Charged Interfaces, Including $\chi^{(3)}$ (ω) Contributions. *Phys. Chem. Chem. Phys.* **2018**, *20* (7), 5190–5199.
- (46) Sun, S.; Schaefer, J.; Backus, E. H. G.; Bonn, M. How Surface-Specific Is 2nd-Order Non-Linear Spectroscopy? *J. Chem. Phys.* **2019**, *151* (23), 230901.
- (47) García Rey, N.; Weißenborn, E.; Schulze-Zachau, F.; Gochev, G.; Braunschweig, B. Quantifying Double-Layer Potentials at Liquid–Gas Interfaces from Vibrational Sum-Frequency Generation. *J. Phys. Chem. C* **2019**, *123* (2), 1279–1286.
- (48) Inoue, K.; Ahmed, M.; Nihonyanagi, S.; Tahara, T. Effect of Hydrogen-Bond on Ultrafast Spectral Diffusion Dynamics of Water at Charged Monolayer Interfaces. *J. Chem. Phys.* **2019**, *150* (5), 054705.
- (49) Prinz, H. Hill Coefficients, Dose–Response Curves and Allosteric Mechanisms. *J. Chem. Biol.* **2010**, *3* (1), 37–44.
- (50) Grahame, D. C. The Electrical Double Layer and the Theory of Electrocapillarity. *Chem. Rev.* **1947**, *41* (3), 441–501.
- (51) Chen, X.; Yang, T.; Kataoka, S.; Cremer, P. S. Specific Ion Effects on Interfacial Water Structure near Macromolecules. *J. Am. Chem. Soc.* **2007**, *129* (40), 12272–12279.
- (52) Johnson, C. M.; Tyrode, E. Study of the Adsorption of Sodium Dodecyl Sulfate (SDS) at the Air/Water Interface: Targeting the

Sulfate Headgroup Using Vibrational Sum Frequency Spectroscopy. *Phys. Chem. Chem. Phys.* **2005**, 7 (13), 2635–2640.

(53) Colthup, N. B.; Daly, L. H.; Wiberley, S. E. *Introduction to Infrared and Raman Spectroscopy*, 2nd ed.; Academic Press: New York, 1975.

(54) Socrates, G. *Infrared and Raman Characteristic Group Frequencies: Tables and Charts*, 3rd ed.; Wiley: New York, 2001.

(55) Davis, A. R.; Oliver, B. G. Raman Spectroscopic Evidence for Contact Ion Pairing in Aqueous Magnesium Sulfate Solutions. *J. Phys. Chem.* **1973**, 77 (10), 1315–1316.

(56) Pye, C. C.; Rudolph, W. W. An Ab Initio and Raman Investigation of Magnesium (II) Hydration. *J. Phys. Chem. A* **1998**, 102 (48), 9933–9943.

(57) Sthoer, A.; Tyrode, E. Interactions of Na^+ Cations with a Highly Charged Fatty Acid Langmuir Monolayer: Molecular Description of the Phase Transition. *J. Phys. Chem. C* **2019**, 123 (37), 23037–23048.

(58) Buchner, R.; Chen, T.; Hefter, G. Complexity in “Simple” Electrolyte Solutions: Ion Pairing in MgSO_4 (Aq). *J. Phys. Chem. B* **2004**, 108 (7), 2365–2375.

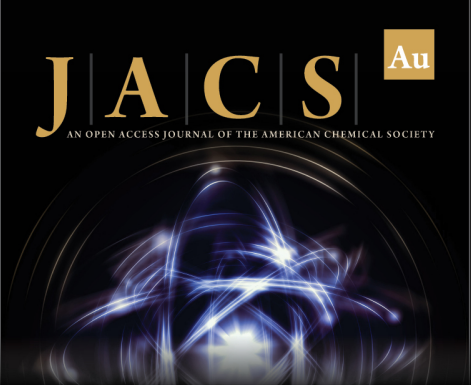
(59) Rudolph, W. W.; Irmer, G.; Hefter, G. T. Raman Spectroscopic Investigation of Speciation in MgSO_4 (Aq). *Phys. Chem. Chem. Phys.* **2003**, 5 (23), 5253–5261.

(60) Casillas-Ituarte, N. N.; Chen, X.; Castada, H.; Allen, H. C. Na^+ and Ca^{2+} Effect on the Hydration and Orientation of the Phosphate Group of DPPC at Air–Water and Air–Hydrated Silica Interfaces. *J. Phys. Chem. B* **2010**, 114 (29), 9485–9495.


(61) Bilkova, E.; Pleskot, R.; Rissanen, S.; Sun, S.; Czogalla, A.; Cwiklik, L.; Róg, T.; Vattulainen, I.; Cremer, P. S.; Jungwirth, P.; Coskun, Ü. Calcium Directly Regulates Phosphatidylinositol 4,5-Bisphosphate Headgroup Conformation and Recognition. *J. Am. Chem. Soc.* **2017**, 139 (11), 4019–4024.

(62) Hollas, J. M. *Modern Spectroscopy*, 4th ed.; John Wiley & Sons: West Sussex, 2004.


(63) Taj, S.; Baird, D.; Rosu-Finsen, A.; McCoustra, M. R. S. Surface Heterogeneity and Inhomogeneous Broadening of Vibrational Line Profiles. *Phys. Chem. Chem. Phys.* **2017**, 19 (11), 7990–7995.




JACS Au
AN OPEN ACCESS JOURNAL OF THE AMERICAN CHEMICAL SOCIETY



Editor-in-Chief
Prof. Christopher W. Jones
Georgia Institute of Technology, USA

Open for Submissions 

pubs.acs.org/jacsau

 **ACS Publications**
Most Trusted. Most Cited. Most Read.